VI. 研究成果の刊行物・別刷

J Neurol (2013) 260:1982–1991
DOI 10.1007/s00415-013-6908-0

ORIGINAL COMMUNICATION

Progressive apraxic agraphia with micrographia presenting as corticobasal syndrome showing extensive Pittsburgh compound B uptake

Yasuhisa Sakurai · Kenji Ishii · Masahiro Sonoo · Yuko Saito · Shigeo Murayama · Atsushi Iwata · Kensuke Hamada · Izumi Sugimoto · Shoji Tsuji · Toru Mannen

Received: 13 December 2012 / Revised: 25 March 2013 / Accepted: 27 March 2013 / Published online: 16 April 2013
© Springer-Verlag Berlin Heidelberg 2013

Abstract A 65-year-old woman developed progressive apraxic agraphia, characterized by poorly formed graphemes, a kanji (Japanese morphograms) recall impairment, relatively preserved oral spelling of kanji characters, and incorrect stroke sequences on writing accompanied by micrographia over a 3-year period. She also showed minor degrees of rigidity, limb-kinetic apraxia, and ideomotor apraxia of the left hand. Although asymmetric rigidity and limb-kinetic apraxia strongly suggested corticobasal degeneration, ^{11}C-Pittsburgh compound B positron emission tomography (PiB-PET) showed the predominantly right-sided accumulation of amyloid β in the cortices and striatum. ^{18}F-fluoro-deoxy-glucose PET and single photon emission computed tomography with a ^{99m}Tc-ethylcysteinate dimer (ECD-SPECT) also revealed predominantly right-sided hypometabolism and hypoperfusion in the primary sensorimotor cortex, posterior cingulate gyrus, temporoparietal cortices, frontal cortices, thalamus, and basal ganglia, a pattern characteristic of both corticobasal degeneration and Alzheimer's disease. The findings suggest that progressive apraxic agraphia with micrographia presenting as corticobasal syndrome can show an Alzheimer's disease pathology. It is also suggested that ideomotor apraxia of the left hand can occur without a callosal lesion, and is caused by hypometabolism or hypoperfusion in the right frontal and parietal cortices, as revealed by PET and SPECT.

Keywords Apraxic agraphia · Non-callosal ideomotor apraxia of the left hand · Micrographia · Corticobasal degeneration · Alzheimer's disease

Y. Sakurai (✉) · K. Hamada · I. Sugimoto · T. Mannen
Department of Neurology, Mitsui Memorial Hospital, 1, Kanda-Izumi-cho, Chiyoda-ku, Tokyo 101-8643, Japan
e-mail: ysakurai-tky@umin.ac.jp

K. Ishii
Positron Medical Center, Tokyo Metropolitan Institute of Gerontology, Tokyo, Japan

M. Sonoo
Department of Neurology, Teikyo University School of Medicine, Tokyo, Japan

Y. Saito
National Center of Neurology and Psychiatry, Tokyo, Japan

S. Murayama
Tokyo Metropolitan Institute of Gerontology, Tokyo, Japan

A. Iwata · S. Tsuji
Department of Neurology, School of Medicine, University of Tokyo, Tokyo, Japan

Introduction

Apraxic agraphia is a writing disorder of motor processing that is responsible for converting orthographic information into neuromuscular commands for handwriting movements [1]. Apraxic agraphia is defined by the following deficits [2]: (1) illegible graphemes in writing that cannot be explained by sensorimotor dysfunction, (2) grapheme production that improves with copying, (3) preserved oral spelling or typing, and (4) incorrect stroke sequences on writing [3, 4]. From a neuropsychological perspective, apraxic agraphia is assumed to result from damage to the parietal graphemic area in which visuokinesthetic and sequential motor engrams for words and letters are stored, or the disconnection of output from the graphemic area to frontal graphic output programming area [2]. When disruption occurs in the graphemic area, patients can recall the orthography of a word, but cannot spell it. In the latter

disconnection-type agraphia, patients can orally spell a character, but cannot specifically write the stroke sequences [3]. The lesion responsible for apraxic agraphia due to focal damage is in the superior parietal lobule or area surrounding the intraparietal sulcus [4, 5].

Apraxic agraphia also occurs in cortical degenerative diseases. This type of progressive apraxic agraphia has been reported in corticobasal syndrome (CBS) [6, 7] or with an unknown etiology [8]. Given that corticobasal degeneration (CBD) predominantly affects the postcentral gyrus and surrounding area asymmetrically, it is not surprising that CBD presents as progressive apraxic agraphia. However, one reported patient exhibited a progranulin mutation related to frontotemporal lobar degeneration [7]. Thus, the etiology of progressive apraxic agraphia appears to be heterogeneous.

Progressive agraphia generally occurs as an initial symptom or manifests in parallel with other language disorders in cortical degeneration, such as Alzheimer's disease (AD) [9–11], frontotemporal lobar degeneration [12], amyotrophic lateral sclerosis [13], and CBD [14]. In AD, lexical agraphia (a selective spelling impairment of irregular or exceptional words) is common, probably because degeneration involves the temporoparietal junction, including the angular gyrus in the early stage, damage to which causes lexical agraphia. Phonological agraphia (a selective spelling impairment of regular or consistent nonwords) [15] and a semantic impairment with homophone confusion [16] are also known to occur in AD. However, apraxic agraphia has rarely been reported in association with AD because the superior parietal lobule, the responsible lesion, is involved in the later stage of AD.

Here, we report a patient with progressive apraxic agraphia who exhibited the clinical features of CBD, but showed prominent Pittsburgh compound B (PiB) uptake in the cortices and striatum on positron emission tomography (PET), and was thus diagnosed with possible AD.

Materials and methods

Patient profile

The patient, a 65-year-old right-handed housewife who graduated from senior high school, found that she could not write some kanji (Japanese morphograms) characters and the characters that she could write became progressively smaller in December 2009. In June 2010, she could not mentally calculate her change when she went shopping. She had no family or past history of neurological disorders. She consulted the Department of Neurology, Teikyo University, Tokyo. MRI and MRA in November 2010 revealed an enlarged right lateral ventricle, bilateral parietal lobe atrophy, diffuse lacunar infarction in the deep white matter (Fig. 1a), and stenosis of the horizontal portion of the right middle cerebral artery (Fig. 1b) and the right fetal type posterior cerebral artery originating from the internal cerebral artery. Single photon emission computed tomography with a ^{99m}Tc-ethylcysteinate dimer (ECD-SPECT) in October 2010 showed hypoperfusion in the bilateral superior parietal region, which was more extensive on the right. Clopidogrel administration was started from November 2010. In December 2010, she could not tie her apron strings at the back, put clothes on properly, or button her shirt. She began to fall easily during walking. Because of her progressive deterioration, she was referred to the Department of Neurology, Mitsui Memorial Hospital, Tokyo, in March 2011. Neurological and neuropsychological examinations showed: (1) agraphia of kanji characters, (2) acalculia, (3) limb-kinetic apraxia of the left hand, (4) dressing apraxia, (5) bilateral (predominantly left-sided) limb ataxia, and (6) minor degrees of lead pipe rigidity in the left hand. She did not show forced grasping, alien hand sign (a feeling that one limb is foreign, with involuntary motor activity [17]), or utilization behavior.

She achieved a lower score for the performance IQ in the Wechsler Adult Intelligence Scale-Revised (WAIS-R) in May 2011 (Table 1). The Western Aphasia Battery (WAB; Japanese edition) administered in May 2011 revealed isolated agraphia, characterized by impaired kanji character recall, poor grapheme formation, a progressive reduction in the character size during writing (micrographia), the deletion of kana (Japanese phonetic writing) characters, and incorrect stroke sequences (Fig. 2). She stopped spelling while writing and resumed writing from the beginning even when the strokes were correct. This kind of trial and error was particularly observed when writing kanji characters. When copying a sentence, she wrote stroke by stroke; referring to the sample and the spelled graphemes barely improved with copying. Her recognition of orally spelled kanji characters was perfect, whereas oral spelling of auditorily presented kanji characters was within the normal range. She also complained that she could not spell out a character, even though she could recall the visual image of the character. She could correctly arrange kanji sequences with character cards that she could not write in response to dictation. Overall, her language profile was rated as apraxic agraphia with micrographia. In praxis, she did not gesture to command the use of a hammer, or copy the examiner gesturing its use with the left hand, but held the actual hammer and used it properly with either hand. Spontaneous drawing of a cube was without perspective, and copying of the cube was inaccurate. She did not show hemispatial neglect or Bálint syndrome.

Subsequent neuropsychological tests, cerebrospinal fluid and apolipoprotein ε genotyping studies, and a positron emission tomography study were conducted between March and October 2011. A follow-up neuropsychological study was performed between April and January 2013. She

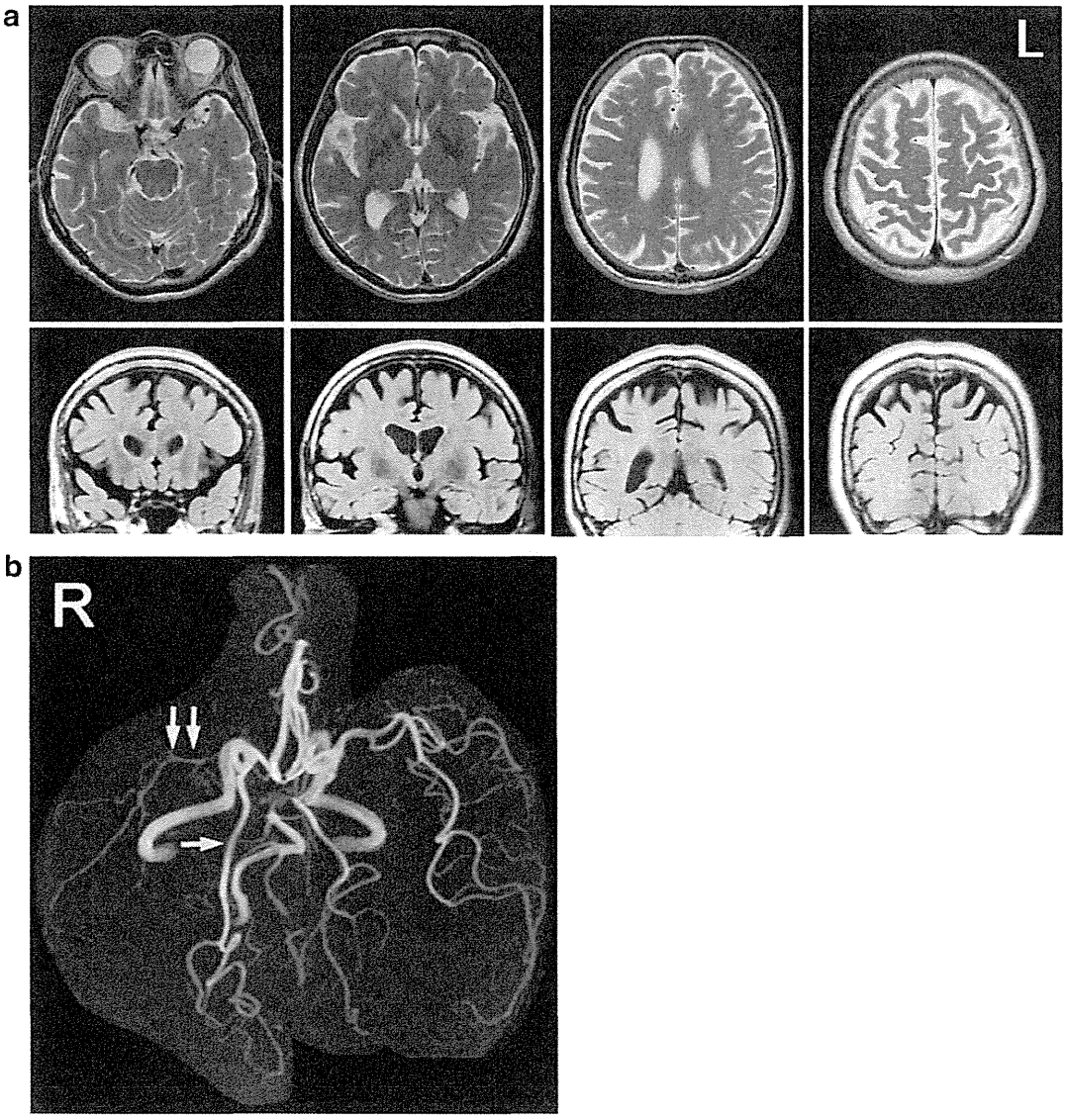

Fig. 1 MRI and MRA of the patient in November 2010. **a** MRI T2-weighted axial and FLAIR coronal images revealed an enlarged right lateral ventricle, bilateral parietal lobe atrophy, and diffuse lacunar infarction in the deep white matter. **b** MRA showed stenosis of the horizontal portion of the right middle cerebral artery (*double arrows*) and right fetal type posterior cerebral artery originating from the internal cerebral artery (*arrow*)

gave written informed consent to each of these studies. The study protocol was approved by the research ethics committee of our hospital, and thus was performed in accordance with the ethical standards laid down in the 1964 Declaration of Helsinki and its later amendments.

Special neuropsychological tests

Reading and writing test

To evaluate the patient's reading and writing performance quantitatively, we conducted a reading and writing test with 100 single-character kanji and kana transcription [18] in March 2011. These characters are taught in the first 3 years of primary school in Japan. The results confirmed the diagnosis of isolated kanji agraphia (Table 1). There were 12 incorrect strokes in kanji and four in kana (Table 2). The trial and error problems described above occurred with 12 kanji and 16 kana characters. Three authors (Y.S, K.H., and I.S.) evaluated the grapheme errors. Among the correct responses, 18 kanji and 15 kana characters were rated as poorly formed, although she complained that all the characters were poorly written. Frequent errors were dislocation (wrong position or direction of each component or stroke) in both kanji and kana.

Table 1 Neuropsychological test scores

Year	2011	2012
WAIS-R		
Verbal IQ	95	93
Digit span forward	6	5
Performance IQ	76	76
WAB		
Spontaneous speech		
Information content (/10)	10	10
Fluency (/10)	10	9
Naming total (/10)	9.4	10
Object naming (/60)	60	60
Repetition (/10)	10	10
Comprehension total (/10)	9.6	9.2
Reading total (/10)	9.7	9.5
Comprehension of sentences (/40)	40	40
Recognition of orally spelled kanji (/6)	6	4
Oral spelling of kanji characters (/6)	3	3
Writing total (/10)	8.15	6.85
Copying of sentences (/10)	8.5[a]	9
Kanji writing from dictation (/6)	2.5	3
Kana writing from dictation (/6)	6	6
Praxis (/10)	rt. 10, lt. 9.7	rt. 10, lt. 9.3
Drawing (/30)	13[a]	16
Calculation (/24)	24	24
100 single-character kanji and kana transcription test (time)		
Kanji reading	100 (2 min 21 s)	100 (2 min 44 s[b])
Kana reading	100 (1 min 10 s)	100 (1 min 24 s)
Kanji writing	56[b] (16 min 34 s[b])	37[b] (24 min 6 s[b])
Kana writing	97[b] (15 min 30 s[b])	88[b] (23 min 3 s[b])
Calculation test		
Mental arithmetic (/40)	28	20
Dictated calculation (/40)	36	37
Electronic calculator (/40)	40	40

[a] More than 2SD below the normal mean [46]

[b] More than 2SD below the normal mean (score) and above the normal mean (time) [4]

An analysis of the visual complexity, concreteness, familiarity, and frequency of the correctly written kanji characters [19] revealed that less complex ($p < 0.001$ by Fisher's exact method), more frequent ($p = 0.0085$ by Fisher's exact method), or more familiar ($p = 0.007$ by Fisher's exact method) characters were written more easily.

Calculation test

As the WAB calculation subtest did not detect acalculia, we performed a supplementary calculation test. The test consisted of an equal number of addition, subtraction, multiplication, and division tasks between two and one digit; half with and half without carrying or borrowing [20]. Mental arithmetic, dictated calculation, and manipulation of an electronic calculator were tested. Mental arithmetic was inferior to dictated calculation (Table 1), which was more attributable to a reduced working memory than to impairment in arithmetic operations.

Test for apraxia

Eight test items were adopted to evaluate limb-kinetic apraxia. The patient could pick up a coin or pencil from a table with her left hand, but it was clumsier than the right hand, and she held a pencil in an awkward manner in her left hand, suggesting slight limb-kinetic apraxia. Furthermore, 10 test items were added to evaluate her use of objects. She had difficulty gesturing and imitating the use of scissors, nail clippers, or a paper fan only with her left hand, whereas the actual use of these tools was preserved. Thus, ideomotor apraxia of the left hand was evident.

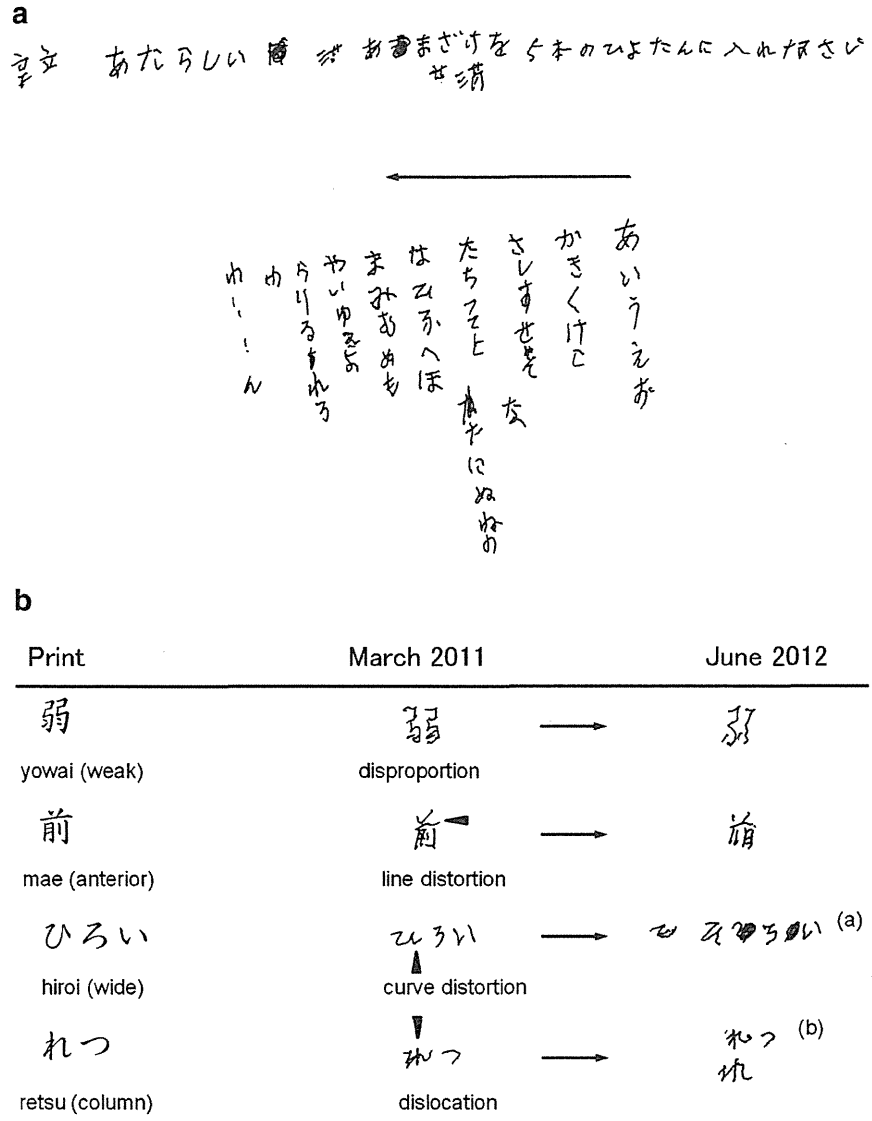

Fig. 2 Patient's writing samples. **a** Writing from the dictation of a sentence (*upper*) showed traces of trial and error, impaired kanji recall (two kanji characters were not recalled), a kana character deletion (ひょうたん a gourd cup → ひょたん), and micrographia. Writing of Japanese syllabary from right to left (*arrow*) also yielded micrographia (*lower*). **b** Examples of grapheme deformities at 1 year and 3 months after the onset and 1 year later. The *arrowhead* denotes the deformed part pointed out by the authors. An evaluation is shown below

Test for cortical tactile disorders

The tactile recognition of objects with blindfolded eyes was normal (right 9/10, left 9/10 of test items). The mean vibration time at the distal interphalangeal joints (DIP) was 14.6 s for the right and 11.4 s for the left: the vibration sense of the left fingers was slightly impaired. There was no left–right difference in two-point discrimination at the tip of the fingers (mean, right 5.4 mm, left 5.8 mm) and graphesthesia at the palm (right 6/10, left 7/10 of trials).

Tests for memory and executive function

Although she did not clinically exhibit amnesia, she could recall only one out of three words in a 5-min delayed recall test, whereas she could recall three visually presented objects completely after 5 min in March 2011. The same result was repeated in January 2013. The Wechsler Memory Scale-Revised test administered in January 2013 (3 years after the disease onset) revealed the following: Verbal Memory Index 77, Visual Memory Index 68, General Memory Index 70, Attention and Concentration 78, and Delayed Recall 79. Thus, her memory remained relatively preserved.

The executive function was evaluated with the Frontal Assessment Battery (FAB) [21] in January 2013. She achieved a score of 15 out of 18. The lost points were similarities (two points) and motor series (Luria's fist-edge-palm test, one point). Her score for lexical fluency was ten (words). No forced grasping, instinctive grasp reaction, such as closing, trapping and magnet response, alien hand sign, or utilization behavior was observed.

Table 2 Types of writing errors and deformities in 100 single-character kanji and kana transcription

Time	March 2011	June 2012
Kanji total errors	44	62
Non-response	13	30
Partial response[a]	13	21
Constructional[a]	14	10
Neographism	0	1
Visual[a]	2	0
Visual/constructional[a]	2	0
Kanji trial and error[b]	12	8
Kanji incorrect stroke sequences[b]	12	17
Kanji deformity total[b]	18	12
Disproportion	2	5
Dislocation	5	4
Line distortion	2	1
Elongation	1	0
Kana total errors	3	12
Non-response	0	1
Partial response	1	1
Constructional	2	9
Neographism	0	1
Kana trial and error[b]	16	20
Kanji incorrect stroke sequences[b]	4	1
Kana deformity total[b]	15	30
Disproportion	1	0
Dislocation	8	5
Line distortion	1	1
Curve distortion	0	4
Elongation	1	0

[a] Partial response. A component of a character was written correctly. Constructional response. Omission or addition of a component of a character. Visual errors. Substitution of another visually similar character, e.g., 角 ([kado], corner) → 負 ([makeru], lose). Visual/constructional errors. Substitution of another visually similar character with the omission or addition of a component of the character

[b] Trial and error and incorrect stroke sequences were evaluated for all characters tested. Trial and error denotes an attempt to write an incorrect or incomplete character repeatedly. Deformity was evaluated only for correct responses. Scores were based on the assessment of the three authors. A character was counted only if two or more authors evaluated the deformity, irrespective of its deformity-type. Deformed characters were chosen when two or more authors' deformity-type assessment was identical. Eventually, the total number of deformities exceeded the sum of each deformity type. Disproportion was the disproportionate size of each component in a character or word, or imbalanced horizontal-to-vertical ratio of a character. Dislocation was the wrong position or direction of each stroke. Distortion was the disruption of a straight line or curve. Elongation was of a line or stroke

Cerebrospinal fluid study and apolipoprotein ε genotyping

The cerebrospinal fluid (CSF) levels of amyloid β 1-42 protein (Aβ), total tau protein (t-tau), and phosphorylated tau-181 protein (p-tau), i.e., standard biomarkers for AD, were measured by ELISA (Innogenetics NV, Zwijndrecht, Belgium) according to the manufacturer's protocol in June 2011. The results revealed that Aβ levels were 632 pg/ml (normal >500), t-tau 1026 pg/ml (normal <300), and p-tau 140 pg/ml (normal <55). Her CSF Aβ concentration was within the normal range, whereas t-tau and p-tau levels were markedly increased. This pattern was exceptional for AD, in which Aβ levels are reduced and t-tau and p-tau levels are elevated [22]. It also differs from that of CBD, in which Aβ levels are decreased and t-tau and p-tau levels are normal [23].

Apolipoprotein ε (ApoE) genotyping was performed with a polymerase chain reaction (PCR) for genomic DNA extracted from the patient's blood sample. The patient was an ε3/ε4 heterozygote.

Neuroimaging study

The patient underwent a follow-up ECD-SPECT at our hospital in April 2011 (Fig. 3). SPECT data were analyzed with statistical parametric mapping (SPM) [24] Version 2. Significance was determined with a two-sample t test for one patient vs. group (normal control) analysis. The normal subject database was provided with the easy Z-score Imaging System (eZIS) version 3 ($n = 18$ for 60–69-year-old women) [25]. Areas showing a significant decrease in cerebral blood flow (uncorrected $p < 0.001$) were shown on standard brain surface images (for details of the method, see Sakurai et al. [19]). Hypoperfusion was noted in the left superior parietal lobule (Brodmann Area 7), right superior and inferior parietal lobules (Areas 7, 39, and 40), right middle occipital gyrus (Area 18), and right superior frontal gyrus (Area 6).

To establish a diagnosis, the patient underwent ^{18}F-2-fluoro-2-deoxy-D-Glucose PET (FDG-PET) and ^{11}C-Pittsburgh compound B PET (PiB-PET) at the Positron Medical Center, Tokyo Metropolitan Institute of Gerontology, Tokyo, in October 2011. FDG and PiB PET image slices were superimposed on the patient's MRI FLAIR axial images with Dr. View software (AJS, Tokyo, Japan). PiB uptake was evaluated with a standardized uptake value ratio (SUVR) taking the cerebellar cortex as a reference region. FDG-PET revealed diffuse cortical hypometabolism other than in the left occipital lobe. The primary sensorimotor cortex, posterior cingulate gyrus, temporoparietal cortices, frontal cortices, thalamus, and basal ganglia were all involved, and it was more pronounced on the right (Fig. 4a). PiB-PET disclosed diffuse and intensive uptake in the bilateral cortices and striatum, with less intensive uptake in the sensorimotor cortex and occipital lobe. Uptake was more marked on the right (Fig. 4b).

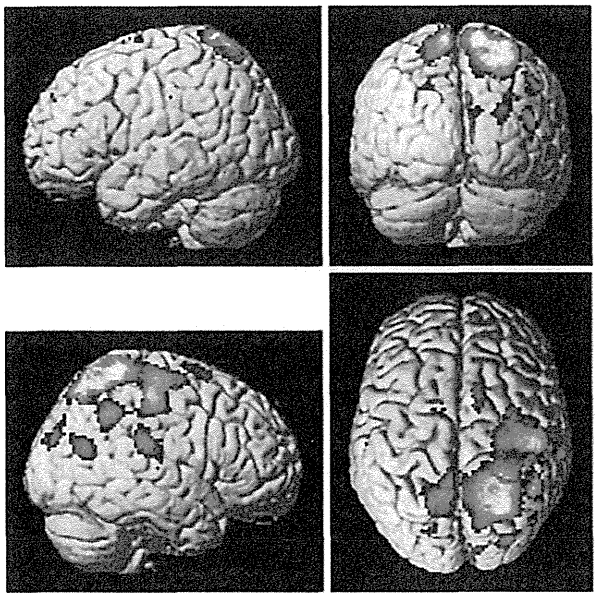

Fig. 3 ^{99m}Tc- ECD SPECT images in April 2011, 1 year and 4 months after the onset. Patient data were compared with those of a normal subject database of the same generation and gender ($n = 22$) with a two-sample t test of SPM2 to show areas with a significant blood flow decrease (uncorrected $p < 0.001$) on standard brain surface images. Hypoperfusion was noted in the left superior parietal lobule, right superior and inferior parietal lobules, right middle occipital gyrus, and right superior frontal gyrus

In August 2011, the patient found that her articulation was poor and myoclonus of the left hand became evident. She was administered donepezil in October 2011. In February 2012, predominantly left-sided rigidity changed from lead pipe to cogwheel. Although she did not go shopping alone and visited our hospital with her husband, she hardly had any difficulties with activities of daily living, except for putting clothes on even 3 years after the onset. Re-examination 1 year later revealed that writing and mental arithmetic had worsened, whereas the general intelligence remained stable (Tables 1, 2). Although she complained that her articulation deteriorated when she spoke for a longer time, only a few phonemic errors (substitution of speech sounds) were noted in the repetition of phoneme sequences such as "pa-ta-ka-pa-ta-ka" (five times) and there was no phonetic distortion (ill-formed phonemes) in spontaneous speech, sentence repetition, or reading in the reassessment using the WAB test. Also, she could stick out her tongue, whistle, and mime blowing out a match. Therefore, neither apraxia of speech nor buccofacial apraxia was noted.

Discussion

The patient developed progressive kanji agraphia with micrographia, acalculia, dressing apraxia, a constructional disorder, and limb-kinetic and ideomotor apraxia of the left hand over a 3-year period. Minor degrees of rigidity were found at the first examination. Agraphia was characterized by poor graphemes, preserved oral spelling, and incorrect stroke sequences. Although the copying of characters did not improve the grapheme forms (which may have been due to a constructional disorder), we can diagnose this disorder as apraxic agraphia. Impaired character recall is sometimes observed in apraxic agraphia [26, 27]; therefore, the coexistence of kanji agraphia due to impaired character recall does not exclude the diagnosis of apraxic agraphia.

Etiological consideration

The patient exhibited limb-kinetic apraxia, ideomotor apraxia, rigidity, and myoclonus of the left hand. Progressive asymmetric rigidity and apraxia, together with a cognitive decline, are consistent with the diagnosis of CBS [28]. FDG-PET revealed hypometabolism in the sensorimotor cortex, thalamus, and basal ganglia, particularly in the right hemisphere, which is characteristic of CBD [29]. However, PiB-PET demonstrated extensive PiB uptake in the neocortex and striatum, which was more prominent on the right. The involvement of the sensorimotor cortex was atypical for AD. However, focal and asymmetric cortical syndromes, such as CBS, have been recognized with an AD pathology that predominantly involves the sensorimotor cortex [30]. Thus, the diagnosis was possible AD (atypical clinical course) with evidence of the AD pathophysiological process [31]. Although multiple lacunes were found on MRI (Fig. 1a), they were too small in size and number to cause the symptoms.

Despite the fact that CSF t-tau and p-tau levels were markedly elevated, Aβ levels were within the normal ranges. The abnormally high CSF t-tau and p-tau levels reflect neuronal degeneration or the formation of tangles in AD [32]. On the other hand, low CSF Aβ levels reflect the deposition of Aβ in plaques [32]. Why our patient had a normal concentration of CSF Aβ with extensive PiB uptake is unclear. However, CSF Aβ values are known to fluctuate by 3–10 % over the course of a day [33]. Also, some patients with AD have normal CSF Aβ levels [34]. Hence, physiological fluctuations, individual differences, and measurement variables may have influenced the result.

A literature review contrasting CBS with an underlying AD pathology (CBS-AD) and that with an underlying CBD pathology (CBS-CBD) [30] revealed that CBS-AD is more strongly associated with a longer disease duration (median 9 vs. 6 years, respectively), a younger age at onset (mean 60 vs. 66 years, respectively), hemisensory neglect, memory impairment, visuospatial difficulties, dressing apraxia, and myoclonus. Our patient was consistent with this view

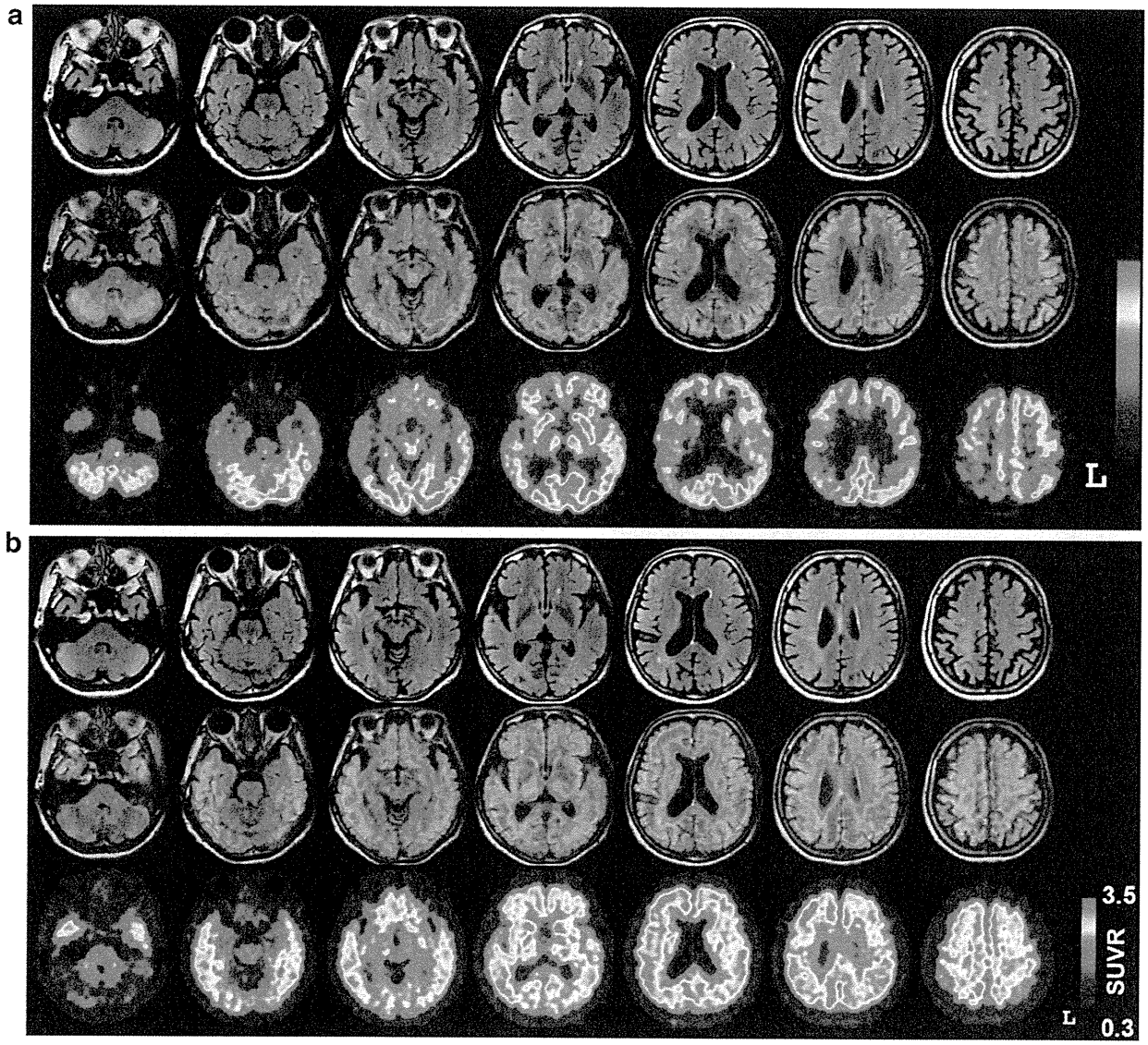

Fig. 4 FDG-PET and PiB-PET images superimposed on the patient's FLAIR images. **a** MRI FLAIR axial images in November 2010 (*upper*), FDG-PET images in October 2011 (*lower*), and PET images superimposed on the patient's FLAIR images (*middle*). FDG-PET revealed diffuse cortical hypometabolism other than in the left occipital lobe, and it was more pronounced on the right. **b** MRI FLAIR axial images in November 2010 (*upper*), PiB-PET images in October 2011 (*lower*), and PET images superimposed on the patient's FLAIR images (*middle*). Diffuse and intensive uptake was observed in the bilateral cortices and basal ganglia, with less intensive uptake in the sensorimotor cortex and occipital lobe. Uptake was more marked on the right. *SUVR* standardized uptake value ratio

of visuospatial difficulties, dressing apraxia, and myoclonus, but she did not show a younger age at onset, hemisensory neglect, or notable memory impairment. In another study [35], initial episodic memory complaints appeared to predict CBS-AD, whereas early frontal-lobe type behavioral symptoms appeared to predict CBS-CBD. However, our patient did not exhibit these symptoms. Therefore, clinical features alone could not be used to predict her pathology. This is because the patient's main lesion was in the predominantly right-sided postrolandic superior parietal cortices, of which the pattern was different from either CBS-CBD or CBS-AD: the patterns of atrophy were noted to be more restricted to posterior frontal regions in CBS-CBD, whereas they were more widespread, including posterior temporal and inferior parietal cortices, in CBS-AD [36].

Substantial evidence has shown that ApoE isoforms differentially affect the aggregation and clearance of Aβ in the brain [37], and the presence of ε4 is associated with increased Aβ in AD [38]. The fact that our patient with one

ApoE ε4 allele showed extensive PiB uptake is consistent with these findings. Clinically diagnosed CBD or CBS [39] encompasses various kinds of neurodegenerative diseases, such as AD, progressive supranuclear palsy, and Pick's disease [40]. The findings in our patient suggest that the asymmetric deposition of Aβ in the striatum and primary sensorimotor cortex can give rise to atypical AD that mimics CBD.

It should be noted that the patient had stenosis of the right middle cerebral artery and right fetal type posterior cerebral artery originating from the internal cerebral artery. It is conceivable that persistent hypoperfusion of the right middle cerebral artery led to Aβ deposition that was more pronounced on the right.

As described in "Introduction", there have been few reports on progressive apraxic agraphia. Our patient demonstrates that AD can present as progressive apraxic agraphia syndrome. Moreover, to the best of our knowledge, apraxic agraphia with micrographia has not been reported. Micrographia is typically observed in Parkinson's syndromes, such as Parkinson's disease, progressive supranuclear palsy [41], and CBD [39], but also occurs with focal damage to the putamen [42] or thalamus [43]. The combination of apraxic agraphia and micrographia suggests the involvement of the parietal cortex, basal ganglia, and thalamus, which was shown by PET and SPECT. It is known that extrapyramidal signs are uncommon in the early stage of AD, but are more prevalent as the disease progresses [44]. It should be noted that the basal ganglia and thalamus can be affected in the early stage of AD and cause parkinsonism.

Non-callosal ideomotor apraxia of the left hand

Ideomotor apraxia commonly manifests bilaterally. If ideomotor apraxia occurs unilaterally in the left hand, it is attributed to callosal disconnection [45]. As our patient did not exhibit any damage to the corpus callosum, the question remains as to why she showed unilateral ideomotor apraxia. Ideomotor apraxia of the left hand without a callosal lesion has already been reported in progressive apraxic agraphia [6]. Since transitive (using tools) action with the right hand was intact, the putative movement representations for skilled acts may have been preserved in the left parietal lobe. A problem occurs when stored movement information is transmitted to the right hemisphere through the corpus callosum. We assume that a "relative callosal disconnection" takes place when the right frontal and parietal lobes are functionally damaged and cannot properly process movement information transmitted from the left parietal lobe, as suggested by PET and SPECT. In any case, it should be noted that ideomotor apraxia of the left hand occurs without a callosal lesion, and this is possible only when there is hypometabolism or hypoperfusion in the right frontal and parietal lobes.

Further studies are needed to elucidate the spectrum of progressive apraxic agraphia and pathogenesis of non-callosal ideomotor apraxia of the left hand.

Acknowledgments The study was partly supported by a Grant-in-Aid for Comprehensive Research on Dementia (No 1103404) from the Ministry of Health, Labour, and Welfare of Japan (K.I.).

Conflicts of interest The authors declare that they have no conflict of interest.

References

1. Rapcsak SZ, Beeson PM (2002) Neuroanatomical correlates of spelling and writing. In: Hillis AE (ed) The handbook of adult language disorders. Integrating cognitive neuropsychology, neurology, and rehabilitation. Psychology Press, New York, pp 71–99
2. Ullrich L, Roeltgen DP (2011) Agraphia. In: Heilman KM, Valenstein E (eds) Clinical neuropsychology, 5th edn. Oxford University Press, New York, pp 130–151
3. Otsuki M, Soma Y, Arai T, Otsuka A, Tsuji S (1999) Pure apraxic agraphia with abnormal writing stroke sequences: report of a Japanese patient with a left superior parietal haemorrhage. J Neurol Neurosurg Psychiatry 66:233–237
4. Sakurai Y, Onuma Y, Nakazawa G, Ugawa Y, Momose T, Tsuji S et al (2007) Parietal dysgraphia: characterization of abnormal writing stroke sequences, character formation, and character recall. Behav Neurol 18:99–114
5. Alexander MP, Fischer RS, Friedman R (1992) Lesion localization in apractic agraphia. Arch Neurol 49:246–251
6. Heilman KM, Coenen A, Kluger B (2008) Progressive asymmetric apraxic agraphia. Cogn Behav Neurol 21:14–17
7. Passov V, Gavrilova RH, Strand E, Cerhan JH, Josephs KA (2011) Sporadic corticobasal syndrome with progranulin mutation presenting as progressive apraxic agraphia. Arch Neurol 68: 376–380
8. Kezuka M, Kawamura M, Yano Y, Shiroyama H (1995) A peculiar kind of agraphia due to degenerative processes predominant in the right hemisphere: comparison with apraxic agraphia. Shinkeishinrigaku 11:196–205
9. Croisile B, Brabant MJ, Carmoi T, Lepage Y, Aimard G, Trillet M (1996) Comparison between oral and written spelling in Alzheimer's disease. Brain Lang 54:361–387
10. Hughes JC, Graham N, Patterson K, Hodges JR (1997) Dysgraphia in mild dementia of Alzheimer's type. Neuropsychologia 35:533–545
11. Rapcsak SZ, Arthur SA, Bliklen DA, Rubens AB (1989) Lexical agraphia in Alzheimer's disease. Arch Neurol 46:65–68
12. Sakurai Y, Tsuchiya K, Oda T, Hori K, Tominaga I, Akiyama H et al (2006) Ubiquitin-positive frontotemporal lobar degeneration presenting with progressive Gogi (word-meaning) aphasia. A neuropsychological, radiological and pathological evaluation of a Japanese semantic dementia patient. J Neurol Sci 250:3–9
13. Ichikawa H, Takahashi N, Hieda S, Ohno H, Kawamura M (2008) Agraphia in bulbar-onset amyotrophic lateral sclerosis: not merely a consequence of dementia or aphasia. Behav Neurol 20:91–99
14. Sakurai Y, Hashida H, Uesugi H, Arima K, Murayama S, Bando M et al (1996) A clinical profile of corticobasal degeneration presenting as primary progressive aphasia. Eur Neurol 36:134–137

15. Platel H, Lambert J, Eustache F, Cadet B, Dary M, Viader F et al (1993) Characteristics and evolution of writing impairment in Alzheimer's disease. Neuropsychologia 31:1147–1158
16. Neils J, Roeltgen DP, Constantinidou F (1995) Decline in homophone spelling associated with loss of semantic influence on spelling in Alzheimer's disease. Brain Lang 49:27–49
17. Doody RS, Jankovic J (1992) The alien hand and related signs. J Neurol Neurosurg Psychiatry 55:806–810
18. Sakurai Y, Sakai K, Sakuta M, Iwata M (1994) Naming difficulties in alexia with agraphia for kanji after a left posterior inferior temporal lesion. J Neurol Neurosurg Psychiatry 57:609–613
19. Sakurai Y, Yagishita A, Goto Y, Ohtsu H, Mannen T (2006) Fusiform type alexia: pure alexia for words in contrast to posterior occipital type pure alexia for letters. J Neurol Sci 247:81–92
20. Sakurai Y, Matsumura K, Iwatsubo T, Momose T (1997) Frontal pure agraphia for kanji or kana: dissociation between morphology and phonology. Neurology 49:946–952
21. Dubois B, Slachevsky A, Litvan I, Pillon B (2000) The FAB: a frontal assessment battery at bedside. Neurology 55:1621–1626
22. Shaw LM, Vanderstichele H, Knapik-Czajka M, Clark CM, Aisen PS, Petersen RC et al (2009) Cerebrospinal fluid biomarker signature in Alzheimer's disease neuroimaging initiative subjects. Ann Neurol 65:403–413
23. Schoonenboom NS, Reesink FE, Verwey NA, Kester MI, Teunissen CE, van de Ven PM et al (2012) Cerebrospinal fluid markers for differential dementia diagnosis in a large memory clinic cohort. Neurology 78:47–54
24. Friston KJ, Holmes AP, Worsley KJ, Poline J-P, Frith CD, Frackowiak RSJ (1995) Statistical parametric maps in functional imaging: a general linear approach. Hum Brain Mapp 2:189–210
25. Matsuda H, Mizumura S, Soma T, Takemura N (2004) Conversion of brain SPECT images between different collimators and reconstruction processes for analysis using statistical parametric mapping. Nucl Med Commun 25:67–74
26. Crary MA, Heilman KM (1988) Letter imagery deficits in a case of pure apraxic agraphia. Brain Lang 34:147–156
27. Levine DN, Mani RB, Calvanio R (1988) Pure agraphia and Gerstmann's syndrome as a visuospatial–language dissociation: an experimental case study. Brain Lang 35:172–196
28. Boeve BF, Lang AE, Litvan I (2003) Corticobasal degeneration and its relationship to progressive supranuclear palsy and frontotemporal dementia. Ann Neurol 54(Suppl 5):S15–S19
29. Ishii K (2002) Clinical application of positron emission tomography for diagnosis of dementia. Ann Nucl Med 16:515–525
30. Hassan A, Whitwell JL, Josephs KA (2011) The corticobasal syndrome-Alzheimer's disease conundrum. Expert Rev Neurother 11:1569–1578
31. McKhann GM, Knopman DS, Chertkow H, Hyman BT, Jack CR Jr, Kawas CH et al (2011) The diagnosis of dementia due to Alzheimer's disease: recommendations from the National Institute on Aging-Alzheimer's Association workgroups on diagnostic guidelines for Alzheimer's disease. Alzheimers Dement 7: 263–269
32. Blennow K, Hampel H (2003) CSF markers for incipient Alzheimer's disease. Lancet Neurol 2:605–613
33. Moghekar A, Goh J, Li M, Albert M, O'Brien RJ (2012) Cerebrospinal fluid Abeta and tau level fluctuation in an older clinical cohort. Arch Neurol 69:246–250
34. Grimmer T, Riemenschneider M, Forstl H, Henriksen G, Klunk WE, Mathis CA et al (2009) Beta amyloid in Alzheimer's disease: increased deposition in brain is reflected in reduced concentration in cerebrospinal fluid. Biol Psychiatry 65:927–934
35. Shelley BP, Hodges JR, Kipps CM, Xuereb JH, Bak TH (2009) Is the pathology of corticobasal syndrome predictable in life? Mov Disord 24:1593–1599
36. Josephs KA, Whitwell JL, Boeve BF, Knopman DS, Petersen RC, Hu WT et al (2010) Anatomical differences between CBS-corticobasal degeneration and CBS-Alzheimer's disease. Mov Disord 25:1246–1252
37. Kim J, Basak JM, Holtzman DM (2009) The role of apolipoprotein E in Alzheimer's disease. Neuron 63:287–303
38. Christensen DZ, Schneider-Axmann T, Lucassen PJ, Bayer TA, Wirths O (2010) Accumulation of intraneuronal Abeta correlates with ApoE4 genotype. Acta Neuropathol 119:555–566
39. Cordato NJ, Halliday GM, McCann H, Davies L, Williamson P, Fulham M et al (2001) Corticobasal syndrome with tau pathology. Mov Disord 16:656–667
40. Boeve BF, Maraganore DM, Parisi JE, Ahlskog JE, Graff-Radford N, Caselli RJ et al (1999) Pathologic heterogeneity in clinically diagnosed corticobasal degeneration. Neurology 53:795–800
41. Williams DR, Holton JL, Strand K, Revesz T, Lees AJ (2007) Pure akinesia with gait freezing: a third clinical phenotype of progressive supranuclear palsy. Mov Disord 22:2235–2241
42. Yoshida T, Yamadori A, Mori E (1989) A case of micrographia with the right hand due to left putaminal infarction. Rinsho Shinkeigaku 29:1149–1151
43. Sakurai Y, Yoshida Y, Sato K, Sugimoto I, Mannen T (2011) Isolated thalamic agraphia with impaired grapheme formation and micrographia. J Neurol 258:1528–1537
44. Scarmeas N, Hadjigeorgiou GM, Papadimitriou A, Dubois B, Sarazin M, Brandt J et al (2004) Motor signs during the course of Alzheimer disease. Neurology 63:975–982
45. Heilman KM, Rothi LJ (2011) Apraxia. In: Heilman KM, Valenstein E (eds) Clinical neuropsychology, 5th edn. Oxford University Press, New York, pp 214–237
46. Sugishita M (1986) The Western Aphasia Battery, Japanese edn. Igaku-Shoin, Tokyo

Downloaded from jnm.snmjournals.org by Kiichi Ishiwata on May 16, 2014. For personal use only.
Journal of Nuclear Medicine, published on April 14, 2014 as doi:10.2967/jnumed.113.133793

Quantitative Analysis of Amyloid Deposition in Alzheimer Disease Using PET and the Radiotracer ^{11}C-AZD2184

Hiroshi Ito[1], Hitoshi Shimada[1], Hitoshi Shinotoh[1], Harumasa Takano[1], Takeshi Sasaki[1], Tsuyoshi Nogami[1], Masayuki Suzuki[1], Tomohisa Nagashima[1], Keisuke Takahata[1], Chie Seki[1], Fumitoshi Kodaka[1], Yoko Eguchi[1], Hironobu Fujiwara[1], Yasuyuki Kimura[1], Shigeki Hirano[1], Yoko Ikoma[1], Makoto Higuchi[1], Kazunori Kawamura[1], Toshimitsu Fukumura[1], Éva Lindström Böö[2], Lars Farde[2], and Tetsuya Suhara[1]

[1]*Molecular Imaging Center, National Institute of Radiological Sciences, Chiba, Japan; and* [2]*AstraZeneca Translational Sciences Center, Department of Clinical Neuroscience, Karolinska Institutet, Stockholm, Sweden*

Characteristic neuropathologic changes in Alzheimer disease (AD) are amyloid-β deposits and neurofibrillary tangles. Recently, a new radioligand for amyloid senile plaques, ^{11}C-labeled 5-(6-{[tert-butyl(dimethyl)silyl]oxy}-1,3-benzothiazol-2-yl)pyridin-2-amine (^{11}C-AZD2184), was developed, and it was reported to show rapid brain uptake followed by rapid washout. In this study, ^{11}C-AZD2184 binding in control subjects and AD patients was examined in more detail by compartment model analysis using a metabolite-corrected arterial input function. The accuracy of simplified quantitative methods using a reference brain region was also evaluated. **Methods:** After intravenous bolus injection of ^{11}C-AZD2184, a dynamic PET scan was obtained for 90 min in 6 control subjects and 8 AD patients. To obtain the arterial input function, arterial blood sampling and high-performance liquid chromatography analysis were performed. **Results:** Time–activity curves in all brain regions could be described using the standard 2-tissue-compartment model. The total distribution volume ratios to reference region (*DVR*) in cerebral cortical regions were significantly higher in AD patients than in control subjects. Although there was no conspicuous accumulation of radioactivity in white matter as compared with other amyloid radioligands, *DVR* values in the centrum semiovale were more than 1 for both control subjects and AD patients, suggesting binding to myelin. The standardized uptake value ratio calculated from integrated time–activity curves in brain regions and the reference region was statistically in good agreement with *DVR*. **Conclusion:** Although the white matter binding of ^{11}C-AZD2184 may have some effect on cortical measurement, it can be concluded that the kinetic behavior of ^{11}C-AZD2184 is suitable for quantitative analysis. The standardized uptake value ratio can be used as a validated measure of ^{11}C-AZD2184 binding in clinical examinations without arterial input function.

Key Words: amyloid; Alzheimer; PET; AZD2184

J Nucl Med 2014; 55:1–7
DOI: 10.2967/jnumed.113.133793

Alzheimer disease (AD) is the most common neurodegenerative disorder. Characteristic neuropathologic changes in AD are amyloid-β deposits and neurofibrillary tangles (*1*). The amyloid cascade hypothesis states that the deposition of amyloid-β drives the remaining Alzheimer pathology, for example, formation of neurofibrillary tangles, cell loss, and vascular damage (*2*). From this perspective, in vivo imaging of amyloid-β deposits may contribute to early diagnosis of AD and serve as a marker for evaluation of disease-modifying drugs. To measure amyloid-β deposits by PET, several radiotracers, for example, ^{11}C-Pittsburgh compound B (^{11}C-PIB) (*3,4*) and (*E*)-4-(2-(6-(2-(2-(2-^{18}F-fluoroethoxy)ethoxy)ethoxy)pyridin-3-yl)vinyl)-*N*-methyl benzenamine (*5*), have been developed and used for examination of the pathophysiology of AD.

^{11}C-labeled 5-(6-{[tert-butyl(dimethyl)silyl]oxy}-1,3-benzothiazol-2-yl)pyridin-2-amine (^{11}C-AZD2184) is a more recently developed radiotracer for amyloid-β deposits. ^{11}C-AZD2184 has been characterized in preclinical studies and has high affinity in vitro for amyloid fibrils (dissociation constant, 8.4 ± 1.0 nM) (*6*). After intravenous injection of ^{11}C-AZD2184 in an initial human study, there was rapid uptake of radioactivity in the brain, followed by rapid washout in control subjects and in AD patients (*7*). The ratios of uptake in cortical regions to a reference brain region devoid of amyloid-β deposition were close to unity in control subjects and high in AD patients. In addition, there was no conspicuous accumulation of radioactivity in white matter.

The initial results indicate that ^{11}C-AZD2184 has potential as a sensitive imaging biomarker for research on the pathophysiology and treatment of AD. The aim of the present study was to examine ^{11}C-AZD2184 binding in greater detail by compartment model analysis using a metabolite-corrected arterial input function. The accuracy of simplified quantitative methods using a reference brain region was also evaluated.

MATERIALS AND METHODS

Subjects

Six control subjects (mean age ± SD, 65 ± 10 y) and 8 AD patients (72 ± 12 y) were recruited (Table 1). All AD patients were diagnosed according to the criteria of the National Institute of Neurologic and Communicative Diseases and Stroke/Alzheimer Disease and Related Disorders Association (*8*). All subjects were characterized according to the Clinical Dementia Rating scale (*9*). The control subjects were rated as 0 by the Clinical Dementia Rating scale, whereas the AD subjects were rated as 0.5, 1, or 2. In addition, the Mini-Mental State Examination was performed in [Table 1]

Received Oct. 10, 2013; revision accepted Jan. 27, 2013.
For correspondence or reprints contact: Hiroshi Ito, Biophysics Program, Molecular Imaging Center, National Institute of Radiological Sciences, 4-9-1 Anagawa, Inage-ku, Chiba 263-8555, Japan.
E-mail: hito@nirs.go.jp
Published online ••••••••••••.
COPYRIGHT © 2014 by the Society of Nuclear Medicine and Molecular Imaging, Inc.

Downloaded from jnm.snmjournals.org by Kiichi Ishiwata on May 16, 2014. For personal use only.

TABLE 1
Profiles of Subjects

Subject group	Subject no.	Age (y)	Sex	Mini-Mental State Examination score	Clinical Dementia Rating scale
Control	NC1	61	F	28	0
	NC2	51	M	29	0
	NC3	60	M	30	0
	NC4	74	M	29	0
	NC5	71	M	28	0
	NC6	75	F	29	0
AD	AD1	76	F	15	1
	AD2	55	F	24	1
	AD3	63	M	13	1
	AD4	75	M	20	0.5
	AD5	84	F	13	1
	AD6	82	F	23	0.5
	AD7	82	F	19	1
	AD8	58	M	13	1

all subjects (*10*). No subject had any observable organic brain lesion according to MR imaging. Control subjects had no cognitive impairment and were free from medications for the central nervous system. The study was approved by the Institutional Review Board of the National Institute of Radiologic Sciences, Chiba, Japan. Written informed consent was obtained from all subjects or from their spouses or other close family members.

Radioligand

^{11}C-AZD2184 was produced according to the literature (*11*). In brief, ^{11}C-AZD2184 was radiosynthesized by reaction of the precursor 5-(6-(tert-butyldimethyl-silyloxy)benzo[d]thiazol-2-yl)pyridin-2-amine with ^{11}C-CH_3I in the presence of potassium hydroxide and subsequent deprotection by water (*7*).

PET Experimental Procedure

All PET measurements were performed with a SET-3000GCT/X scanner (Shimadzu Corp.) (*12*), which provides 99 sections with an axial field of view of 26 cm. The intrinsic spatial resolution is 3.4 mm in-plane and 5.0 mm in full width at half maximum axially. Images were reconstructed by the filtered backprojection algorithm. With a gaussian filter (cutoff frequency, 0.3 cycle/pixel), the reconstructed in-plane resolution was 7.5 mm in full width at half maximum. Data were acquired in 3-dimensional mode. Scatter correction was done by a hybrid scatter-correction method based on acquisition with dual-energy window setting (*13*). A 4-min transmission scan using a ^{137}Cs line source was obtained to correct for attenuation.

After intravenous bolus injection of ^{11}C-AZD2184 over 1 min, a dynamic PET scan was obtained for 90 min. The frame sequence consisted of six 10-s, three 20-s, six 1-min, four 3-min, and fourteen 5-min frames. The radioactivity injected was 380 ± 12 and 380 ± 13 MBq, and the specific radioactivity was 131 ± 38 and 119 ± 28 GBq/μmol at the time of injection for control subjects and AD patients, respectively.

To obtain the arterial input function, 32 samples of arterial blood were taken after injection. The fraction of radioactivity representing unchanged ^{11}C-AZD2184 in plasma was determined by high-performance

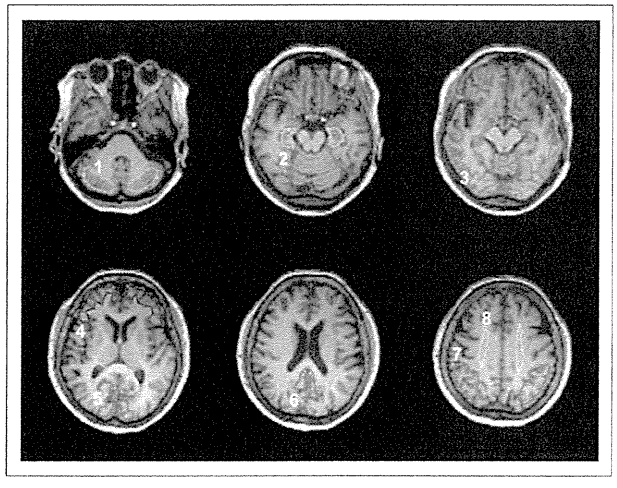

FIGURE 1. ROIs drawn on coregistered MR images. ROIs are defined for cerebellar cortex (1), parahippocampal gyrus including hippocampus (2), lateral side of temporal cortex (3), base side of frontal cortex (4), cuneus of occipital cortex (5), posterior region of cingulate gyrus (6), parietal cortex (7), and centrum semiovale (8).

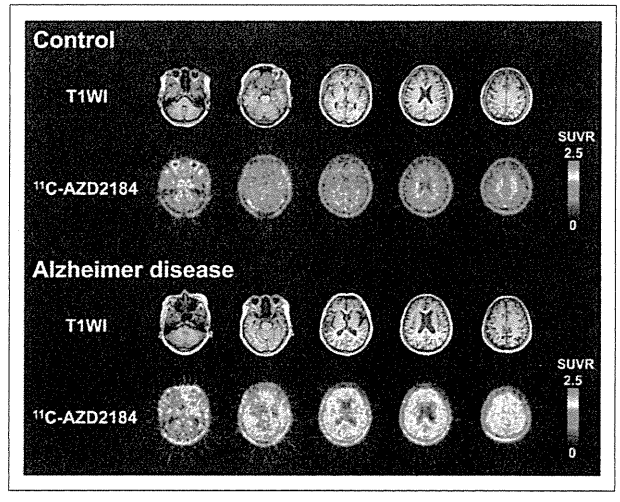

FIGURE 2. Representative *SUVR* images of ^{11}C-AZD2184 binding in control subject and AD patient. Integration interval was 40–60 min. Corresponding MR images (T1-weighted [T1WI]) are shown. Scale maximum and minimum values are 2.5 and 0 of *SUVR*. All images are transaxial sections, and anterior is at top of image and subjects' right is at left.

Downloaded from jnm.snmjournals.org by Kiichi Ishiwata on May 16, 2014. For personal use only.

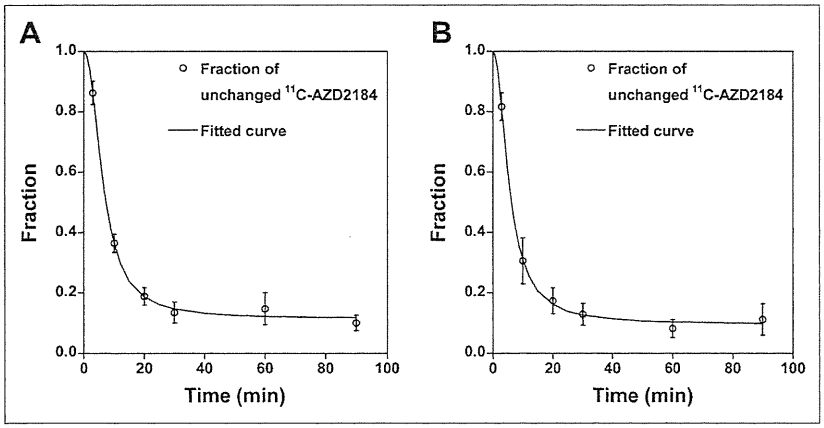

FIGURE 3. Time courses of fraction of radioactivity representing unchanged ^{11}C-AZD2184 in plasma for control subjects (A) and AD patients (B). Values are mean ± SD. Fitted curves were obtained using Hill equation.

liquid chromatography from 6 blood samples for each subject. Acetonitrile was added to each plasma sample, and the samples were then centrifuged. The obtained supernatant was subjected to radio–high-performance liquid chromatography analysis (column, μBondapak [10 μm, 7.8 × 300 nm]; Waters) (mobile phase, 90% acetonitrile [A]/1 mol/L ammonium formate [B]; gradient, 0–10 min [A/B], 22/78–47/53, 10–11 min [A/B], 47/53–80/20, and 11–12 min [A/B], 80/20–22/78; isocratic, 12–15 min end; flow rate, 6.0 mL/min). Plasma protein binding was not determined in the present study. The time curves for the fraction of unchanged ^{11}C-AZD2184 in plasma were fitted by the Hill equation and used for kinetic analysis.

MR Imaging Procedure

All MR imaging examinations were performed with a 3-T MR scanner (GE Healthcare). Three-dimensional volumetric acquisition of a T1-weighted 3-dimensional fast spoiled gradient-recalled acquisition in the steady-state sequence produced a gapless series of thin transverse sections (echo time, 2.848 ms; repetition time, 6.992 ms; prep time, 900 ms; flip angle, 8°; field of view, 260 mm; acquisition matrix, 256 × 256; slice thickness, 1 mm; scan time, 367 s). Proton density–weighted and T2-weighted images were obtained by a 2-dimensional double-echo fast spin echo sequence with interleaved and gapless acquisition (echo time for proton density–weighted images, 10.58 ms; effective echo time for T2-weighted images, 95.22 ms; repetition time, 3,000.00 ms; field of view, 240 mm; acquisition matrix, 256 × 256; slice thickness, 3 mm [no gap, interleave]; echo train length, 16; scan time, 309 s). T1-weighted images were used for analysis of PET images. Proton density–weighted and T2-weighted images were used to confirm whether subjects had any observable organic brain lesion.

Regions of Interest (ROIs)

All MR images were coregistered to the individual PET images using the software package PMOD (version 3.0; PMOD Technologies Ltd.). ROIs were drawn on coregistered MR images (T1-weighted images) and transferred to the PET images. ROIs were defined for the cerebellar cortex, parahippocampal gyrus including the hippocampus, posterior region of the cingulate gyrus, base side of the frontal cortex, lateral side of the temporal cortex, parietal cortex, cuneus of the occipital cortex, and centrum semiovale (Fig. 1). Each ROI was drawn on 3 adjacent sections, and data were pooled to obtain the average radioactivity concentration for the whole volume of interest. To obtain regional time–activity curves, regional radioactivity was calculated for each frame, corrected for decay, and plotted versus time. [Fig. 1]

Kinetic Model for Interpretation of ^{11}C-AZD2184 Binding

To interpret the kinetic behavior of ^{11}C-AZD2184, the standard 2-tissue-compartment model with 4 first-order rate constants was used (*14*). The rate constants K_1 and k_2 describe the influx and efflux rates for radiotracer diffusion through the blood–brain barrier, respectively. The rate constants k_3 and k_4 describe the radiotracer transfer between the compartments for nondisplaceable radiotracer and specific binding. The distribution volume with only nondisplaceable binding in a brain region (V_{ND}), the total distribution volume (V_T), and the binding potential relative to the concentration of nondisplaceable radiotracer in brain (BP_{ND}) are expressed as follows (*15*):

$$V_{ND} = \frac{K_1}{k_2} \quad \text{Eq. 1}$$

$$V_T = \frac{K_1}{k_2}\left(1 + \frac{k_3}{k_4}\right) \quad \text{Eq. 2}$$

$$BP_{ND} = \frac{k_3}{k_4} \quad \text{Eq. 3}$$

Kinetic Analysis of ^{11}C-AZD2184 Binding

To estimate the rate constants (K_1, k_2, k_3, and k_4), nonlinear curve fitting was performed in a least-squares sense to the regional time–activity curves (*16*). In this analysis, the blood volume, which depends on the first-pass extraction fraction of the tracer, was assumed to be 0.04 mL/mL to diminish the influence of tracer remaining in the blood using the radioactivity of whole blood (*17*). The radioactivity of unchanged ^{11}C-AZD2184

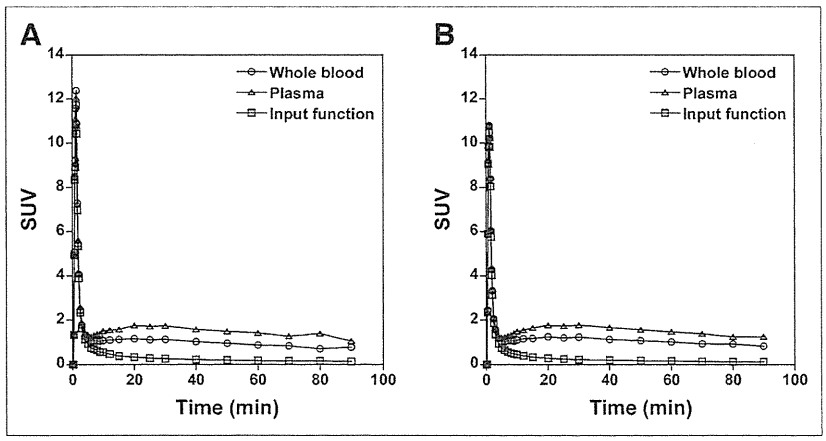

FIGURE 4. Time courses of average radioactivity concentration in arterial whole blood and plasma for control subjects (A) and AD patients (B). Time courses of average radioactivity concentration of unchanged ^{11}C-AZD2184 in plasma (i.e., arterial input function) are also shown.

Downloaded from jnm.snmjournals.org by Kiichi Ishiwata on May 16, 2014. For personal use only.

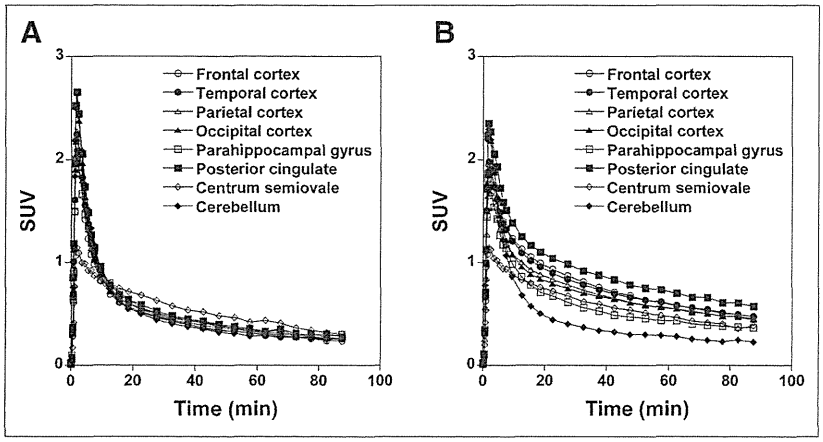

FIGURE 5. Average time–activity curves for brain regions in control subjects (A) and AD patients (B).

in plasma was used as the arterial input function. For this analysis, PMOD was used. V_T was calculated from the rate constants as an indicator of amyloid-β deposits (Eq. 2).

Quantitative Approach Using Reference Region

The cerebellum has been suggested as a reference brain region because no fibrillar amyloid plaques have been demonstrated in this region postmortem (*18,19*). A quantitative approach, taking advantage of the cerebellum as a reference region, can be used to calculate the total distribution volume ratio (*DVR*) as follows:

$$DVR = V_{T(brain)}/V_{T(cerebellum)}, \quad \text{Eq. 4}$$

where $V_{T(brain)}$ and $V_{T(cerebellum)}$ are total distribution volume in brain regions and the cerebellum, respectively. The BP_{ND} is equal to $DVR - 1$ if the cerebellum is the ideal reference brain region.

In addition, the standardized uptake value (*SUV*) was calculated from the time-integrated regional radioactivity concentration normalized with injected dose per body weight. The integration intervals were 20–40, 40–60, and 60–90 min. The integration interval of 20–40 min includes the peak equilibrium condition (*20*), and the integration intervals of 40–60 and 60–90 min correspond to the late part of the time–activity curve. In a simplified approach and because the cerebellum can be used as a reference brain region, the *SUV* ratio (*SUVR*) indicating amyloid-β deposits was calculated using the following expression:

$$SUVR = SUV_{brain}/SUV_{cerebellum}, \quad \text{Eq. 5}$$

where SUV_{brain} and $SUV_{cerebellum}$ represent the *SUV* in brain regions and the cerebellum, respectively.

RESULTS

In this study, no adverse event was observed after intravenous injection of ^{11}C-AZD2184. Representative *SUVR* images showing the distribution of brain radioactivity after intravenous injection of ^{11}C-AZD2184 are shown for a control subject and an AD patient [Fig. 2] in Figure 2. There was no conspicuous accumulation of radioactivity in white matter, the same as in a previous report (*7*). In AD patients, radioactivity in the cerebral cortices was higher than in the control subjects. By visual assessment of the *SUVR* images, all control subjects appeared negative with regard to specific binding of ^{11}C-AZD2184, whereas all AD patients appeared positive.

The time courses for the average fraction of radioactivity representing unchanged ^{11}C-AZD2184 in plasma for control subjects and AD patients are shown in Figure 3. [Fig. 3] Sixty minutes after injection of ^{11}C-AZD2184, the fraction of radioactivity representing unchanged ^{11}C-AZD2184 in plasma was 0.11–0.12. The time courses of the average radioactivity concentration in whole blood and plasma and the time course of the radioactivity concentration of unchanged ^{11}C-AZD2184 in plasma (i.e., arterial input function) are shown in Figure 4. [Fig. 4]

The regional time–activity curves for control subjects and AD patients are shown in Figure 5. At 18.5, 37.5, 57.5, and 87.5 min after injection of [Fig. 5] ^{11}C-AZD2184, the ratios of regional radioactivity of posterior cingulate to cerebellum were 1.14 ± 0.03, 1.21 ± 0.09, 1.27 ± 0.17, and 1.08 ± 0.27 for control subjects and 2.19 ± 0.22, 2.60 ± 0.57, 2.55 ± 0.49, and 2.52 ± 0.64 for AD patients. In control subjects, radioactivity concentrations in cerebral cortical regions were similar to those for the cerebellum at the end of data acquisition, the same as in a previous report (*7*). In AD patients, radioactivity concentrations in cerebral cortical regions were higher than in the cerebellum.

Typical time–activity curves in brain regions of an AD patient and the corresponding fitted curves obtained by kinetic analyses are shown in Figure 6. The time–activity curves in all brain [Fig. 6] regions could be described by the standard 2-tissue-compartment model.

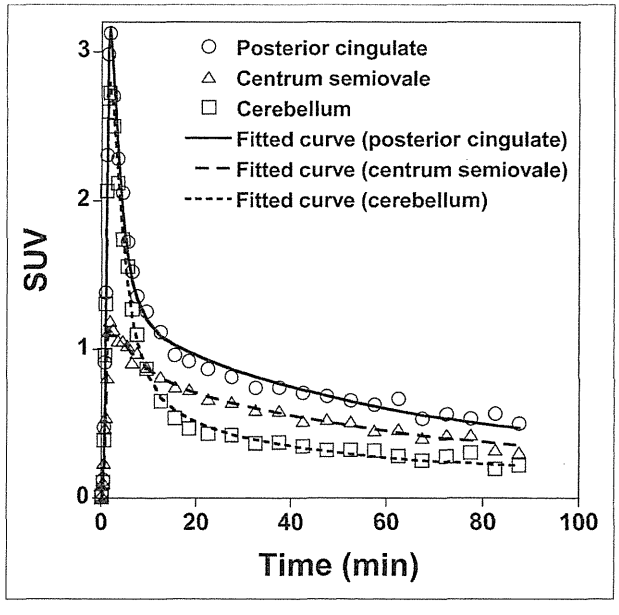

FIGURE 6. Typical time–activity curves in brain regions of AD patient and fitted curves obtained using standard 2-tissue-compartment model.

jnm133793-pm ■ 4/7/14

Downloaded from jnm.snmjournals.org by Kiichi Ishiwata on May 16, 2014. For personal use only.

TABLE 2
Kinetic Parameters Obtained by 2-Tissue-Compartment Model Analysis of ^{11}C-AZD2184 Binding in Control Subjects

Brain region	K_1 (mL/mL/min)	k_2 (min^{-1})	k_3 (min^{-1})	k_4 (min^{-1})	V_T (mL/mL)	*DVR*
Frontal cortex	0.23 ± 0.07	0.42 ± 0.09	0.05 ± 0.02	0.05 ± 0.02	1.14 ± 0.19	0.99 ± 0.07
Temporal cortex	0.25 ± 0.07	0.42 ± 0.09	0.06 ± 0.02	0.05 ± 0.02	1.22 ± 0.17	1.07 ± 0.06
Parietal cortex	0.25 ± 0.06	0.43 ± 0.08	0.05 ± 0.02	0.05 ± 0.02	1.18 ± 0.17	1.03 ± 0.09
Occipital cortex	0.32 ± 0.07	0.53 ± 0.12	0.05 ± 0.02	0.04 ± 0.01	1.28 ± 0.17	1.12 ± 0.09
Hippocampus	0.22 ± 0.05	0.41 ± 0.12	0.08 ± 0.04	0.06 ± 0.02	1.27 ± 0.19	1.11 ± 0.07
Posterior cingulate	0.32 ± 0.09	0.52 ± 0.11	0.06 ± 0.03	0.06 ± 0.03	1.33 ± 0.23	1.16 ± 0.11
Centrum semiovale	0.09 ± 0.03	0.17 ± 0.08	0.09 ± 0.04	0.05 ± 0.01	1.50 ± 0.31	1.30 ± 0.12
Cerebellum	0.28 ± 0.06	0.38 ± 0.05	0.03 ± 0.02	0.05 ± 0.02	1.15 ± 0.22	—

Values are mean ± SD.

The rate constants and related kinetic parameters for ^{11}C-AZD2184 binding in control subjects and AD patients are given [Table 2] in Tables 2 and 3, respectively. In control subjects, the V_T in [Table 3] cerebral cortical regions was similar to that in the cerebellum. In AD patients, V_T values were consistently higher in cerebral cortical regions than in the cerebellum. The V_T and the *DVR* in cerebral cortical regions were significantly higher in AD patients than in control subjects (unpaired *t* test, $P < 0.01$). The *DVR* in the centrum semiovale was more than 1 in average for both control subjects and AD patients. No significant differences in V_T and *DVR* were observed for the centrum semiovale between control subjects and AD patients.

The *SUVR* and *DVR* in control subjects and AD patients are [Table 4] shown in Table 4. The *SUVR* for each integration interval was at the same level and in agreement with the corresponding *DVR* value. *SUVR* and *DVR* in cerebral cortical regions were significantly higher in AD patients than in control subjects. The relation- [Fig. 7] ship between *DVR* and *SUVR* is shown in Figure 7. Significant correlations were observed between *DVR* and *SUVR* for each integration interval.

DISCUSSION

In the present examination of ^{11}C-AZD2184 binding to amyloid-β deposits, there was high binding in the cerebral cortical regions of AD patients in comparison with control subjects, the same as in a previous report (*7*). The *DVR* values of ^{11}C-AZD2184 in cerebral cortical regions for both control subjects and AD patients were almost the same level as those of ^{11}C-PIB reported previously (*18*). Although previously developed radioligands, such as ^{11}C-PIB, show high nonspecific binding in white matter, the white matter binding was not conspicuous for ^{11}C-AZD2184. The *SUV*s in the white matter were less than 0.5 after 60 min of injection of ^{11}C-AZD2184 in both control subjects and AD patients, and those of ^{11}C-PIB were reported to be more than 1 (*4*). The regional time–activity curves could be described by the standard 2-tissue-compartment model. The dissociation rate constant k_4 was 0.04–0.05 min^{-1}, not zero, indicating reversibility of binding. Thus, it was evident that the kinetic behavior of ^{11}C-AZD2184 is similar to that of established neuroreceptor ligands such as ^{11}C-raclopride (*20*) and that this radioligand is likely suitable for quantitative analyses using various established approaches.

The white matter binding of ^{11}C-AZD2184 appears lower than that reported for other amyloid radioligands such as ^{11}C-PIB (*4*), the same as in the previous autoradiographic study with postmortem brain (*6*). In control subjects, there was no obvious difference between binding in gray and white matter. However, kinetic analysis revealed the *DVR* to be more than 1 (~1.3–1.5) in the centrum semiovale, a region that almost entirely consists of white matter, for both control subjects and AD patients. The nature of the binding of amyloid ligand to white matter is not fully understood. It has been reported that ^{11}C-PIB may bind to myelin, which is organized in a β-sheet structure in the same way as amyloid-β deposits (*21–23*). The proposed binding has low affinity and is likely not saturable because of the large amount of myelin in the brain. In other words, a high concentration of unlabeled ligand would be required to saturate the binding of amyloid

TABLE 3
Kinetic Parameters Obtained by 2-Tissue-Compartment Model Analysis of ^{11}C-AZD2184 Binding in AD Patients

Brain region	K_1 (mL/mL/min)	k_2 (min^{-1})	k_3 (min^{-1})	k_4 (min^{-1})	V_T (mL/mL)	*DVR*
Frontal cortex	0.21 ± 0.04	0.27 ± 0.08	0.09 ± 0.02	0.04 ± 0.01	2.49 ± 0.48	1.96 ± 0.25
Temporal cortex	0.22 ± 0.05	0.27 ± 0.09	0.08 ± 0.01	0.04 ± 0.01	2.48 ± 0.43	1.97 ± 0.26
Parietal cortex	0.18 ± 0.05	0.25 ± 0.10	0.07 ± 0.02	0.04 ± 0.01	2.30 ± 0.47	1.84 ± 0.37
Occipital cortex	0.28 ± 0.05	0.39 ± 0.10	0.07 ± 0.02	0.03 ± 0.01	2.35 ± 0.54	1.86 ± 0.33
Hippocampus	0.21 ± 0.03	0.32 ± 0.08	0.07 ± 0.02	0.04 ± 0.02	1.81 ± 0.33	1.43 ± 0.15
Posterior cingulate	0.26 ± 0.06	0.30 ± 0.10	0.08 ± 0.02	0.04 ± 0.01	3.04 ± 0.77	2.39 ± 0.42
Centrum semiovale	0.10 ± 0.02	0.14 ± 0.03	0.08 ± 0.05	0.05 ± 0.03	1.94 ± 0.54	1.51 ± 0.22
Cerebellum	0.28 ± 0.05	0.37 ± 0.08	0.03 ± 0.02	0.06 ± 0.05	1.27 ± 0.20	—

Values are mean ± SD.

Downloaded from jnm.snmjournals.org by Kiichi Ishiwata on May 16, 2014. For personal use only.

TABLE 4
*SUVR*s of ^{11}C-AZD2184 in Control Subjects and AD Patients

	Control				AD			
	SUVR				*SUVR*			
Brain region	20–40 min*	40–60 min*	60–90 min*	*DVR*	20–40 min*	40–60 min*	60–90 min*	*DVR*
Frontal cortex	1.04 ± 0.04	1.07 ± 0.09	0.99 ± 0.10	0.99 ± 0.07	2.16 ± 0.28†	2.17 ± 0.27†	2.13 ± 0.28†	1.96 ± 0.25†
Temporal cortex	1.10 ± 0.04	1.14 ± 0.04	1.08 ± 0.07	1.07 ± 0.06	2.09 ± 0.23†	2.14 ± 0.25†	2.15 ± 0.30†	1.97 ± 0.26†
Parietal cortex	1.06 ± 0.07	1.08 ± 0.10	1.03 ± 0.09	1.03 ± 0.09	1.93 ± 0.30†	1.98 ± 0.38†	2.01 ± 0.44†	1.84 ± 0.37†
Occipital cortex	1.13 ± 0.06	1.21 ± 0.08	1.11 ± 0.10	1.12 ± 0.09	1.87 ± 0.38†	1.97 ± 0.33†	2.01 ± 0.38†	1.86 ± 0.33†
Hippocampus	1.15 ± 0.07	1.18 ± 0.05	1.15 ± 0.07	1.11 ± 0.07	1.52 ± 0.11†	1.52 ± 0.15†	1.58 ± 0.16†	1.43 ± 0.15†
Posterior cingulate	1.19 ± 0.08	1.24 ± 0.13	1.17 ± 0.12	1.16 ± 0.11	2.46 ± 0.44†	2.54 ± 0.43†	2.56 ± 0.42†	2.39 ± 0.42†
Centrum semiovale	1.41 ± 0.08	1.49 ± 0.14	1.36 ± 0.17	1.30 ± 0.12	1.68 ± 0.19	1.72 ± 0.21	1.64 ± 0.22	1.51 ± 0.22

*Integration interval.
†Significant differences from normal control subjects (unpaired *t* test, $P < 0.01$).
Values are mean ± SD.

radioligands to cerebral white matter (*24*). Moreover, it has been estimated that ROIs defined for the cerebral cortex contain about 60% of gray matter and 30% of white matter (*25*). This tissue heterogeneity may affect ^{11}C-AZD2184 binding in the cerebral cortices.

To examine simplified approaches for quantification of ^{11}C-AZD2184 binding, the *SUVR* was calculated using the cerebellum as a reference brain region, with integration intervals of 20–40, 40–60, and 60–90 min. The *SUVR* of each integration interval was at the same level and statistically in good agreement with the *DVR* values obtained by kinetic analysis, although systemic overestimations in *SUVR* were observed. This cross-validation indicates that ^{11}C-AZD2184 binding can be estimated using a short scanning time and no arterial blood sampling. The nonlinearity and bias of *SUVR* as compared with *DVR* are observed in most radiotracers (*26,27*). However, the fast relative equilibrium of ^{11}C-AZD2184 could be one of the main advantages over ^{11}C-PIB (*4*). In further study, systemic errors in *SUVR* of ^{11}C-AZD2184 should be investigated with simulation studies. Although all integration intervals can be used to calculate *SUVR*, integration intervals of 40–60 and 60–90 min might be more preferable because the early part of the time–activity curve is generally affected by changes in K_1 due to changes in cerebral blood flow (*20*). However, a lack of an early phase of PET data might hamper an adequate coregistration between PET and MR images, especially in control subjects because of a low binding in the white matter.

It has been reported that synaptic loss is associated with nondiffuse plaques, but not with diffuse plaques (*28*), and that the neuropathology in AD is characterized by cortical neuritic plaque containing dense-cored amyloid deposition (*29*). ^{11}C-BF227, a recently developed radiotracer for in vivo imaging of amyloid-β, has been considered to bind more preferentially to dense-cored amyloid deposition than ^{11}C-PIB (*19*). Further research is needed to demonstrate the binding characteristics of ^{11}C-AZD2184 in different types of amyloid plaque.

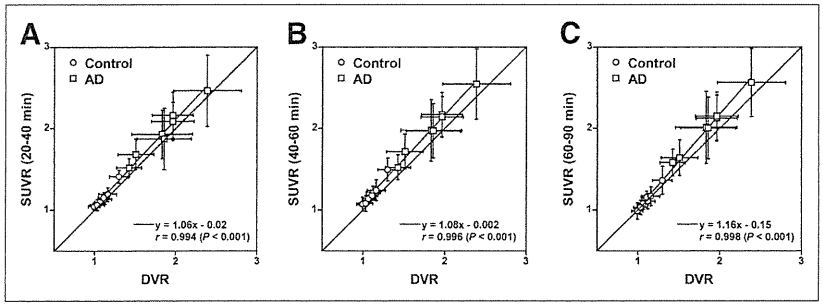

FIGURE 7. Relationship between *DVR* and *SUVR* for integration intervals of 20–40 min (A), 40–60 min (B), and 60–90 min (C). Respective data indicate mean and SD of each ROI.

CONCLUSION

The novel radioligand ^{11}C-AZD2184 provides high-contrast imaging of amyloid-β deposits in brain. The regional kinetics of ^{11}C-AZD2184 binding in control subjects and AD patients could be described by the standard 2-tissue-compartment model. The *SUVR* calculated from integrated time–activity curves in targeted and reference brain regions can be used as an index of ^{11}C-AZD2184 binding for clinical investigations without arterial input function.

DISCLOSURE

The costs of publication of this article were defrayed in part by the payment of page charges. Therefore, and solely to indicate this fact, this article is hereby marked "advertisement" in accordance with 18 USC section 1734. This study was supported in part by the "Japan Advanced Molecular Imaging Program (J-AMP)" of the Ministry of Education, Culture, Sports, Science and Technology (MEXT), Japanese Government, and a grant-in-aid for Comprehensive Research on Dementia (no. 11103404) from the Ministry of Health, Labor and Welfare. No other potential conflict of interest relevant to this article was reported.

ACKNOWLEDGMENTS

We thank Katsuyuki Tanimoto, Takahiro Shiraishi, Kazuko Suzuki, and Izumi Izumida for their assistance in the PET experiments. 5-(6-{[tert-butyl(dimethyl)silyl]oxy}-1,3-benzothiazol-2-yl)pyridin-2-amine (AZD2184) and its precursor 5-(6-(tert-butyldimethylsilyloxy)benzo[d]thiazol-2-yl)pyridin-2-amine were kindly provided by AstraZeneca R&D, Södertälje, Sweden.

Downloaded from jnm.snmjournals.org by Kiichi Ishiwata on May 16, 2014. For personal use only.

REFERENCES

1. Braak H, Braak E. Neuropathological stageing of Alzheimer-related changes. *Acta Neuropathol.* 1991;82:239–259.
2. Hardy JA, Higgins GA. Alzheimer's disease: the amyloid cascade hypothesis. *Science.* 1992;256:184–185.
3. Mathis CA, Wang Y, Holt DP, Huang GF, Debnath ML, Klunk WE. Synthesis and evaluation of ^{11}C-labeled 6-substituted 2-arylbenzothiazoles as amyloid imaging agents. *J Med Chem.* 2003;46:2740–2754.
4. Klunk WE, Engler H, Nordberg A, et al. Imaging brain amyloid in Alzheimer's disease with Pittsburgh compound-B. *Ann Neurol.* 2004;55:306–319.
5. Choi SR, Golding G, Zhuang Z, et al. Preclinical properties of ^{18}F-AV-45: a PET agent for Aβ plaques in the brain. *J Nucl Med.* 2009;50:1887–1894.
6. Johnson AE, Jeppsson F, Sandell J, et al. AZD2184: a radioligand for sensitive detection of beta-amyloid deposits. *J Neurochem.* 2009;108:1177–1186.
7. Nyberg S, Jonhagen ME, Cselenyi Z, et al. Detection of amyloid in Alzheimer's disease with positron emission tomography using [^{11}C]AZD2184. *Eur J Nucl Med Mol Imaging.* 2009;36:1859–1863.
8. McKhann G, Drachman D, Folstein M, Katzman R, Price D, Stadlan EM. Clinical diagnosis of Alzheimer's disease: report of the NINCDS-ADRDA Work Group under the auspices of Department of Health and Human Services Task Force on Alzheimer's Disease. *Neurology.* 1984;34:939–944.
9. Morris JC. The Clinical Dementia Rating (CDR): current version and scoring rules. *Neurology.* 1993;43:2412–2414.
10. Folstein MF, Folstein SE, McHugh PR. "Mini-mental state": a practical method for grading the cognitive state of patients for the clinician. *J Psychiatr Res.* 1975;12:189–198.
11. Andersson JD, Varnas K, Cselenyi Z, et al. Radiosynthesis of the candidate beta-amyloid radioligand [^{11}C]AZD2184: positron emission tomography examination and metabolite analysis in cynomolgus monkeys. *Synapse.* 2010;64:733–741.
12. Matsumoto K, Kitamura K, Mizuta T, et al. Performance characteristics of a new 3-dimensional continuous-emission and spiral-transmission high-sensitivity and high-resolution PET camera evaluated with the NEMA NU 2-2001 standard. *J Nucl Med.* 2006;47:83–90.
13. Ishikawa A, Kitamura K, Mizuta T, et al. Implementation of on-the-fly scatter correction using dual-energy window method in continuous 3D whole body PET scanning. *IEEE Nucl Sci Symp Conf Rec.* 2005;5:2497–2500.
14. Mintun MA, Raichle ME, Kilbourn MR, Wooten GF, Welch MJ. A quantitative model for the in vivo assessment of drug binding sites with positron emission tomography. *Ann Neurol.* 1984;15:217–227.
15. Innis RB, Cunningham VJ, Delforge J, et al. Consensus nomenclature for in vivo imaging of reversibly binding radioligands. *J Cereb Blood Flow Metab.* 2007;27:1533–1539.
16. Marquardt D. An algorithm for least-squares estimation of nonlinear parameters. *J Soc Ind Appl Math.* 1963;11:431–441.
17. Ito H, Ota M, Ikoma Y, et al. Quantitative analysis of dopamine synthesis in human brain using positron emission tomography with L-[β-^{11}C]DOPA. *Nucl Med Commun.* 2006;27:723–731.
18. Price JC, Klunk WE, Lopresti BJ, et al. Kinetic modeling of amyloid binding in humans using PET imaging and Pittsburgh compound-B. *J Cereb Blood Flow Metab.* 2005;25:1528–1547.
19. Kudo Y, Okamura N, Furumoto S, et al. 2-(2-[2-dimethylaminothiazol-5-yl] ethenyl)-6- (2-[fluoro]ethoxy)benzoxazole: a novel PET agent for in vivo detection of dense amyloid plaques in Alzheimer's disease patients. *J Nucl Med.* 2007;48:553–561.
20. Ito H, Hietala J, Blomqvist G, Halldin C, Farde L. Comparison of the transient equilibrium and continuous infusion method for quantitative PET analysis of [^{11}C]raclopride binding. *J Cereb Blood Flow Metab.* 1998;18:941–950.
21. Klunk WE, Wang Y, Huang GF, et al. The binding of 2-(4'-methylaminophenyl) benzothiazole to postmortem brain homogenates is dominated by the amyloid component. *J Neurosci.* 2003;23:2086–2092.
22. Klunk WE, Lopresti BJ, Ikonomovic MD, et al. Binding of the positron emission tomography tracer Pittsburgh compound-B reflects the amount of amyloid-beta in Alzheimer's disease brain but not in transgenic mouse brain. *J Neurosci.* 2005;25:10598–10606.
23. Fodero-Tavoletti MT, Rowe CC, McLean CA, et al. Characterization of PiB binding to white matter in Alzheimer disease and other dementias. *J Nucl Med.* 2009;50:198–204.
24. Stankoff B, Freeman L, Aigrot MS, et al. Imaging central nervous system myelin by positron emission tomography in multiple sclerosis using [methyl-^{11}C]-2-(4'-methylaminophenyl)- 6-hydroxybenzothiazole. *Ann Neurol.* 2011;69:673–680.
25. Ito H, Takahashi H, Arakawa R, Takano H, Suhara T. Normal database of dopaminergic neurotransmission system in human brain measured by positron emission tomography. *Neuroimage.* 2008;39:555–565.
26. Ito H, Halldin C, Farde L. Localization of 5-HT$_{1A}$ receptors in the living human brain using [carbonyl-^{11}C]WAY-100635: PET with anatomic standardization technique. *J Nucl Med.* 1999;40:102–109.
27. Zhou Y, Sojkova J, Resnick SM, Wong DF. Relative equilibrium plot improves graphical analysis and allows bias correction of standardized uptake value ratio in quantitative ^{11}C-PiB PET studies. *J Nucl Med.* 2012;53:622–628.
28. Masliah E, Terry RD, Mallory M, Alford M, Hansen LA. Diffuse plaques do not accentuate synapse loss in Alzheimer's disease. *Am J Pathol.* 1990;137:1293–1297.
29. Price JL. Diagnostic criteria for Alzheimer's disease. *Neurobiol Aging.* 1997;18:S67–S70.

Sato et al. EJNMMI Research 2013, 3:76
http://www.ejnmmires.com/content/3/1/76

EJNMMI Research
a SpringerOpen Journal

ORIGINAL RESEARCH Open Access

Noninvasive k_3 estimation method for slow dissociation PET ligands: application to [^{11}C] Pittsburgh compound B

Koichi Sato[1,2], Kiyoshi Fukushi[1], Hitoshi Shinotoh[1,3], Hitoshi Shimada[1,4], Shigeki Hirano[1,5], Noriko Tanaka[6], Tetsuya Suhara[1], Toshiaki Irie[1] and Hiroshi Ito[1*]

Abstract

Background: Recently, we reported an information density theory and an analysis of three-parameter plus shorter scan than conventional method (3P+) for the amyloid-binding ligand [^{11}C]Pittsburgh compound B (PIB) as an example of a non-highly reversible positron emission tomography (PET) ligand. This article describes an extension of 3P + analysis to noninvasive '3P++' analysis (3P + plus use of a reference tissue for input function).

Methods: In 3P++ analysis for [^{11}C]PIB, the cerebellum was used as a reference tissue (negligible specific binding). Fifteen healthy subjects (NC) and fifteen Alzheimer's disease (AD) patients participated. The k_3 (index of receptor density) values were estimated with 40-min PET data and three-parameter reference tissue model and were compared with that in 40-min 3P + analysis as well as standard 90-min four-parameter (4P) analysis with arterial input function. Simulation studies were performed to explain k_3 biases observed in 3P++ analysis.

Results: Good model fits of 40-min PET data were observed in both reference and target regions-of-interest (ROIs). High linear intra-subject (inter-15 ROI) correlations of k_3 between 3P++ (*Y*-axis) and 3P + (*X*-axis) analyses were shown in one NC ($r^2 = 0.972$ and slope = 0.845) and in one AD ($r^2 = 0.982$, slope = 0.655), whereas inter-subject k_3 correlations in a target region (left lateral temporal cortex) from 30 subjects (15 NC + 15 AD) were somewhat lower ($r^2 = 0.739$ and slope = 0.461). Similar results were shown between 3P++ and 4P analyses: $r^2 = 0.953$ for intra-subject k_3 in NC, $r^2 = 0.907$ for that in AD and $r^2 = 0.711$ for inter-30 subject k_3. Simulation studies showed that such lower inter-subject k_3 correlations and significant negative k_3 biases were not due to unstableness of 3P++ analysis but rather to inter-subject variation of both k_2 (index of brain-to-blood transport) and k_3 (not completely negligible) in the reference region.

Conclusions: In [^{11}C]PIB, the applicability of 3P++ analysis may be restricted to intra-subject comparison such as follow-up studies. The 3P++ method itself is thought to be robust and may be more applicable to other non-highly reversible PET ligands with ideal reference tissue.

Keywords: [^{11}C]Pittsburgh compound B; Alzheimer's disease; Kinetic modeling; PET quantification; Reference tissue; Slow dissociation ligand

* Correspondence: hito@nirs.go.jp
[1]Molecular Imaging Center, National Institute of Radiological Sciences, 4-9-1 Anagawa, Inage-ku, Chiba 260-8555, Japan
Full list of author information is available at the end of the article

Springer

© 2013 Sato et al.; licensee Springer. This is an Open Access article distributed under the terms of the Creative Commons Attribution License (http://creativecommons.org/licenses/by/2.0), which permits unrestricted use, distribution, and reproduction in any medium, provided the original work is properly cited.

Background

Various reversible-type radioligands have been developed for *in vivo* neuroreceptor study with positron emission tomography (PET). Both arterial blood sampling and long dynamic PET scan, up to 120 min, are required for standard nonlinear least-squares (NLS) analysis to estimate K_1 to k_4 in the two-tissue compartment four-parameter model (4P model): K_1 represents the blood-to-brain transport constant, k_2 represents the brain-to-blood transport constant, k_3 represents the first-order association rate constant for specific binding, and k_4 represents the dissociation rate constant for specific binding. The k_3 represents $B_{max}{\cdot}k_{on}$, where B_{max} is maximum receptor density and k_{on} is the *in vivo* association rate constant. Since k_3 represents available receptors for the PET ligand, it is the target parameter of major interest in most PET studies. However, quantification of k_3 in the 4P model is often difficult because of uncertainty of the k_4 estimate and high correlation between the k_3 and k_4 estimates. As surrogate parameters for B_{max}, binding potential and distribution volume have been widely used [1-4]. Several reference tissue methods have also been developed [5-10].

Irreversible (enzyme-substrate type) radiotracers [^{11}C] methylpiperidin-4-yl acetate and propionate have been developed for the measurement of cerebral acetylcholine esterase activity using PET [11,12]. In this case the two-tissue compartment three-parameter (K_1 to k_3) model (3P model) was used to estimate k_3, which is an index of acetylcholine esterase activity. In the 3P model, the precision of k_3 estimate is usually higher than in the 4P model, in spite of shorter PET scan time (40 to 60 min), since there is no need of k_4 estimation in the 3P model.

We have previously defined two mathematical functions, the information density function and information function, which are useful for model selection and optimization of scan time in PET [13]. Based on simulations using both functions, we proposed a new method (3P + method) for quantification of k_3 for moderately reversible ligands. '3P+' means three-parameter model plus short PET scan. In this method, the 3P model ($k_4 = 0$ model) was applied to the early-phase PET data (up to 30 to 40 min) from reversible ligands with moderate k_4 (moderately reversible ligands). Although the 3P + method was not always developed for a specific ligand, the amyloid-binding radiotracer [^{11}C]Pittsburgh compound B (PIB) was used as an example for the moderately reversible ligands (k_4 = 0.018/min). The 3P + method afforded a more stable k_3 estimate than the standard 90-min 4P analysis. However, there is still the drawback of the necessity for arterial blood sampling and radiometabolite analysis, which may restrict the widespread use of this method in daily clinical practice.

In this article, we propose a noninvasive 3P++ analysis using [^{11}C]PIB. 3P++ means 3P + analysis plus use of a reference tissue for input function. To validate the proposed method, the linear correlations of k_3 estimates were evaluated between 40-min 3P++ and 3P + analyses, as well as between 3P++ and 90-min 4P analyses in clinical PET studies. In addition, simulation studies were performed to explain k_3 biases observed in the 3P++ analysis.

Methods

Theory

Assumptions in 3P++ analysis

The following are assumptions used in 3P++ analysis:

- Assumption 1 (on the nature of radioligand used): We apply 3P++ analysis only to moderately reversible or nearly irreversible radioligands ($k_4 \le 0.03$/min), but exclude highly reversible ligands. [^{11}C]PIB is an example of moderately reversible ligands (k_4 = 0.018/min).
- Assumption 2 (on the duration time of PET scan): We use early-phase PET data in the curve fitting. In [^{11}C]PIB, dynamic PET data during 0 to 40 min was described well with the 3P model, since the effect of the k_4 process on PET data was negligible within these early-phase kinetics [13].
- Assumption 3 (on the specific binding in the reference tissue, k_{3r}): Specific binding of radioligand is negligible in the reference tissue ($k_{3r} = 0$). In [^{11}C]PIB, the gray matter of the cerebellum is usually used as a reference tissue for input function [14]. We apply the one-tissue compartment two-parameter (K_1, k_2) model (2P model) to the reference tissue.

Working equation for 3P++ analysis

The working equation for the 3P++ analysis has been reported [15]:

$$\begin{aligned} C_t(t) &= R_1\left[\delta(t) + \frac{k_{2r}k_3}{k_2+k_3} + \left(k_{2r} - k_2 - \frac{k_{2r}k_3}{k_2+k_3}\right)e^{-(k_2+k_3)t}\right] \otimes C_r(t) \\ &= R_1 C_r(t) + \frac{R_1 k_{2r} k_3}{k_2+k_3}\int_0^t C_r(\tau)d\tau - \frac{R_1 k_2(k_2+k_3-k_{2r})}{k_2+k_3} \\ &\quad \times \int_0^t e^{-(k_2+k_3)(t-\tau)} C_r(\tau)d\tau, \end{aligned} \tag{1}$$

where $C_t(t)$ is the radioactivity concentration in the target tissue and $C_r(t)$ is that in the reference tissue; k_{2r} is the k_2 in the reference tissue and $\otimes$ is the convolution integral. The rate of tracer penetration into the target tissue is obtained as the relative value R_1, which is the ratio of target K_1 to reference K_1.

Clinical PET study

Human subjects

Two groups of subjects, a normal control (NC) group and an Alzheimer's disease (AD) group, participated in